COMPDYN 2011
ECCOMAS Thematic Conference on
Computational Methods in Structural Dynamics and Earthquake Engineering
M. Papadrakakis, M. Fragiadakis, V. Plevris (eds.)
Corfu, Greece, 25-28 May 2011

SEARCHING FOR LOCAL CONTACT CONSTRAINTS BY THE QUASI-NEWTON METHODS IN THE FINITE ELEMENT PROCEDURES FOR CONTACT-IMPACT PROBLEMS

Dušan Gabriel[1], Ján Kopačka[1], Jiří Plešek[1] and Miran Ulbin[2]

[1]Institute of Thermomechanics
Academy of Sciences of the Czech Republic
Dolejškova 5
182 00 Praha 8, Czech Republic
e-mail: {gabriel,kopacka,plesek}@it.cas.cz

[2] Faculty of Mechanical Engineering
University of Maribor
Smetanova 17
2000 Maribor, Slovenia
e-mail: ulbin@uni-mb.si

Keywords: FEM, Contact-Impact Problems, Local Contact Search, Quasi-Newton Methods

Abstract. *The essential part of the solution of a contact problem in the finite element method is to locate probable contact areas reliably and efficiently. Most contact searching algorithms are based on the definition of master and slave contact surfaces, when the slave nodes/integration points are checked on against master segments for penetration. The present paper deals with the local search problem which comprises the calculation of the exact position of the slave node/integration point with respect to a given master segment. Since the analytical solution for finding the distance does not exist for a general quadrilateral contact segment, the iterative numerical procedure is solved. Several methods for the solution of non-linear algebraic systems are tested: the Newton-Raphson procedure, the least square projection, the steepest descent method, Broydens method, BFGS method, DFP method and the simplex method. The effectiveness of methods is tested by means of a contact-impact problem of two colliding thick plates, for which analytical solution is available.*

1 INTRODUCTION

The key issue in the numerical treatment of contact problem in the finite element method is to locate contact areas reliably and efficiently. Most contact algorithms are based on the master-slave concept, when the position of slave node is checked on against the master segment for penetration. The contact detection can be usually divided into two phases: the global search for finite elements/segments which actually intersect and the local search for projections of slave points (nodes/quadrature points) onto master surfaces.

An overview of global search algorithms might be found in Refs. [1, 2]. When the global search is successfully done, the local search is performed. There are several possibilities to deal with this problem.

The most frequently used approach for local contact searching is described in Ref. [3]. The contact point is defined on the master segment as the point closest to the slave point. Its parametric coordinates are calculated by solving the minimization problem. There is an analytical solution for linear triangular segments, however, a bilinear quadrilateral as well as higher order elements have to be solved numerically. The Newton-Raphson method is applied for solving the simple non-linear equations.

In order to increase efficiency, in Ref. [4] each quadrilateral segment is broken into four triangles with their common vertex at the centre of the master segment. The contact point is calculated by determining which triangle is closest to the slave node and projecting the slave node onto it. Although efficiency of this approach is undeniable, it is not adequate for distorted elements which can occur within post-buckling calculations [5].

For node-to-segment contact design the algorithm based on the definition of a mesh normal was proposed in Ref. [6]. The mesh normal vector of a node is defined as the average normal vector for all surfaces which adjacent to the node. The inside-outside algorithm [7] employs this vector to determine whether the projection of a node is located inside or outside of a surface. Since no iterations are involved the algorithm is very fast. However, a lack of continuity on the boundary of surfaces called the deadzone problem was observed. In order to overcome this drawback, the free-form-surface (FFS) algorithm was proposed in Ref. [2]. The contact area is approximated with the FFS patch, which ensures smoothness. The accuracy can be increased by subdividing of the surface patch.

In this paper, we focused on the solution of a minimization problem between slave integration (quadrature) point and the master segment of the three-dimensional quadratic serendipity element. The solution of resulting non-linear equations is not trivial, especially when higher order finite elements are taken into account. First, the formulation of a minimization problem is presented in Section 2. Various numerical methods for the solution of this problem are presented in Section 3. First, the convergence difficulties of the Newton-Raphson method are analyzed. Next, the least square projection constructed as the linearized Newton-Raphson scheme [5] is mentioned. Then, the line search strategy is presented [8], utilized in the steepest descent method, Broyden's method, BFGS and DFP method [9]. The last three methods belong to an alternative approach to the Newton-Raphson method, known as quasi-Newton methods. Finally, the Nelder-Mead simplex method [10] is discussed as an interesting alternative to preceding methods. The effectiveness of methods is compared in Section 3.9, followed by the numerical example of the longitudinal impact of two thick plates in Section 4.

2 FORMULATION OF THE MINIMIZATION PROBLEM

Let us consider the slave quadrature point $\mathbf{y}_s \in \mathbb{E}^3$ and the master segment γ_c. The aim of the local contact search is to calculate the parametric coordinates $\xi_1, \xi_2 \in [-1, 1]$ corresponding to projection $\bar{\mathbf{y}}(\xi_1, \xi_2) \in \mathbf{E^3}$ of the quadrature point $\mathbf{y}_s$ (see Fig. 1).

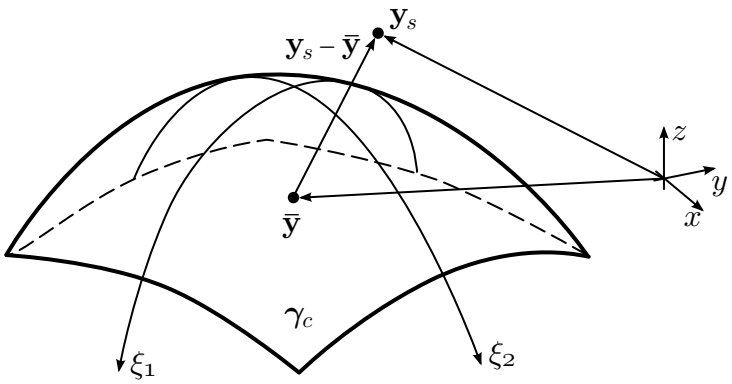

Figure 1: Formulation of the minimization problem.

Such a point has to satisfy

$$\bar{\mathbf{y}} = \min_{\mathbf{y} \in \gamma_c} \{(\mathbf{y}_s - \mathbf{y}) \cdot (\mathbf{y}_s - \mathbf{y})\} \tag{1}$$

where the minimization of the inner product on $\mathbb{E}^3$ instead of more natural Euclidean norm has been used. Hence, the minimized function is defined as

$$f = (\mathbf{y}_s - \mathbf{y}) \cdot (\mathbf{y}_s - \mathbf{y}) \tag{2}$$

The necessary condition for local extremum is

$$\begin{aligned} (\mathbf{y}_s - \mathbf{y}) \cdot \frac{\partial \mathbf{y}}{\partial \xi_1} &= 0 \\ (\mathbf{y}_s - \mathbf{y}) \cdot \frac{\partial \mathbf{y}}{\partial \xi_2} &= 0 \end{aligned} \tag{3}$$

The master segment γ_c is parametrized by

$$\mathbf{y}(\xi_1, \xi_2) = \sum_{i=1}^{n} N_i(\xi_1, \xi_2) \mathbf{Y}_i \tag{4}$$

where $N_i(\xi_1, \xi_2) : \mathbb{R} \times \mathbb{R} \to \mathbb{R}$ are the shape functions, n is the number of nodes and $\mathbf{Y}_i \in \mathbb{E}^3$ are the global coordinates of nodes. Note that the partial derivations are constant and Eqn. (3) is system of linear equations for linear triangular segments. If higher order elements are taken into account, Eqn. (3) results in the system of non-linear algebraic equations. The inequality constraints $|\xi_1|, |\xi_2| \leq 1$ for isoparametric segment γ_c are not explicitly imposed. The solution of the unconstrained problem lying outside the permissible range indicates that the integration point does not penetrate onto the master segment. Therefore, methods for unconstrained optimization can be employed [8, 9].

3 METHODS FOR UNCONSTRAINED OPTIMIZATION

For the purpose of this section, some notation will be introduced. First, the vector of the isoparametric coordinates is defined as

$$\mathbf{x}^k = \left\{ \begin{array}{c} \xi_1^k \\ \xi_2^k \end{array} \right\} \tag{5}$$

where the superscript k is the iteration counter. Then, the gradient of the minimized function is denoted by

$$\nabla f^k = \left\{ \begin{array}{c} (\mathbf{y}_s - \mathbf{y}) \cdot \dfrac{\partial \mathbf{y}}{\partial \xi_1} \\ \\ (\mathbf{y}_s - \mathbf{y}) \cdot \dfrac{\partial \mathbf{y}}{\partial \xi_2} \end{array} \right\} \tag{6}$$

and the Hessian matrix of second partial derivations is

$$\mathbf{H}^k = \left[\begin{array}{cc} \dfrac{\partial^2 f^k}{\partial \xi_1^2} & \dfrac{\partial^2 f^k}{\partial \xi_1 \partial \xi_2} \\ \\ \dfrac{\partial^2 f^k}{\partial \xi_1 \partial \xi_2} & \dfrac{\partial^2 f^k}{\partial \xi_2^2} \end{array} \right] \tag{7}$$

3.1 Newton-Raphson method

The numerical scheme of the Newton-Raphsons method is based on the first-order Taylor's series expansion of (3) about $\mathbf{x}^k$. The numerical scheme can be written in the form

$$\mathbf{x}^{k+1} = \mathbf{x}^k - \left(\mathbf{H}^k\right)^{-1} \cdot \nabla f^k \tag{8}$$

Generally, there are two constructions of the Newton-Raphson method. First, the method can be thought as the root-finding algorithm of the residuals (3). The matrix $\mathbf{H}^k$ is considered as the tangent matrix and the point $\mathbf{x}^k + 1$ is understood as the intersection of hyperplanes with constraint $f\left(\mathbf{x}^k\right) = 0$. Second, the Newton-Raphson is taken as an quadratic interpolation in point $\mathbf{x}^k$

$$Q = \frac{1}{2}\left(\mathbf{H}^k \cdot \Delta \mathbf{x}^k\right) \cdot \Delta \mathbf{x}^k + \nabla f^k \cdot \Delta \mathbf{x}^k + f^k, \qquad \Delta \mathbf{x}^k = \mathbf{x}^{k+1} - \mathbf{x}^k \tag{9}$$

Then, new iteration $\mathbf{x}^{k+1}$ is minimizer of this quadratic function

$$\mathbf{H}^k \cdot \Delta \mathbf{x}^k + \nabla f^k = 0 \tag{10}$$

Indeed, for convex functions the Newton-Raphson produces only positive definite matrices $\mathbf{H}^k$, for which the quadratic function (9) is paraboloid. Minimization of such interpolation embodies quadratic convergence [8]. On the other hand, for general non-linear functions the positive definiteness of $\mathbf{H}^k$ cannot be guaranteed. In case of indefinite Hessian matrix, next iteration $\mathbf{x}^k$ could bounce, because hyperbolic paraboloid, which represents indefinite matrix, could have the minimimum (saddle point) far from $\mathbf{x}^{k+1}$. Consequently, the solution could converge to another local minimum or even diverge. The necessary condition for the convergence of the Newton-Raphson method is positive definiteness of the Hessian matrix $\mathbf{H}^k$. The rigorous proof can be found in [8]. It should be pointed out that the convergence property of the Newton-Raphson iteration is difficult to achieve since the Hessian matrix of the distance function (2) to be minimized is not positive definite in general. Therefore, several methods will be discussed in the following sections.

3.2 Least squares projection

Whereas the Newton-Raphson linearizes the minimized function (2), the least squares projection linearizes the master contact segment (4)

$$\mathbf{y} = \mathbf{y}^k + \left.\frac{\partial \mathbf{y}}{\partial \mathbf{x}}\right|_{\mathbf{x}^k} \cdot \Delta \mathbf{x}^k \tag{11}$$

For given point $\mathbf{x}^k$ the necessary condition for local extremum (3) becomes linear

$$\left(\mathbf{y}_s - \mathbf{y}^k + \left.\frac{\partial \mathbf{y}}{\partial \mathbf{x}}\right|_{\mathbf{x}^k} \cdot \Delta \mathbf{x}^k\right) \cdot \left.\frac{\partial \mathbf{y}}{\partial \mathbf{x}}\right|_{\mathbf{x}^k} = 0 \tag{12}$$

By rearranging

$$\left.\frac{\partial \mathbf{y}}{\partial \mathbf{x}}\right|_{\mathbf{x}^k} \cdot \left.\frac{\partial \mathbf{y}}{\partial \mathbf{x}}\right|_{\mathbf{x}^k} \cdot \Delta \mathbf{x}^k = - \left.\frac{\partial \mathbf{y}}{\partial \mathbf{x}}\right|_{\mathbf{x}^k} \cdot \left(\mathbf{y}_s - \mathbf{y}^k\right) \tag{13}$$

and introducing the matrix notation, we obtain

$$\left\{ \begin{array}{c} \dfrac{\partial \mathbf{y}^k}{\partial \xi_1} \\ \\ \dfrac{\partial \mathbf{y}^k}{\partial \xi_2} \end{array} \right\} \cdot \left\{ \begin{array}{cc} \dfrac{\partial \mathbf{y}^k}{\partial \xi_1} & \dfrac{\partial \mathbf{y}^k}{\partial \xi_2} \end{array} \right\} \cdot \left\{ \begin{array}{c} \Delta \xi_1^k \\ \\ \Delta \xi_2^k \end{array} \right\} = - \left\{ \begin{array}{c} \dfrac{\partial \mathbf{y}^k}{\partial \xi_1} \\ \\ \dfrac{\partial \mathbf{y}^k}{\partial \xi_2} \end{array} \right\} \cdot \left\{\mathbf{y}_s - \mathbf{y}^k\right\} \tag{14}$$

Benson et al. [5] recommends three iterations of this method to generate an initial guess for the Newton-Raphson. We try to use the least squares projection as fully-fledged method. The global convergence was attained for arbitrary initial guess [11]. Nevertheless, the global minimum lies outside the permissible range in most cases and therefore this method is not feasible for local search.

3.3 Line search strategy

In each iteration of a line search method a search direction is computed $\mathbf{p}^k \in \mathbb{R}^n$ and then decided how far to move along that direction. The iteration is given by

$$\mathbf{x}^{k+1} = \mathbf{x}^k + t^k \mathbf{p}^k \tag{15}$$

where the positive scalar $t^k \in \mathbb{R}$ is called the step length. The success of a line search method depends on the effective choices of both the direction $\mathbf{p}^k$ and the step length parameter t^k. Most line-search algorithms require $\mathbf{p}^k$ to be a descent direction for which $\mathbf{p}^k \cdot \nabla f^k < 0$. The search direction often has the form

$$\mathbf{p}^k = -\mathbf{D}^k \cdot \nabla f^k \tag{16}$$

where $\mathbf{D}^k \in \mathbb{R}^{n,n}$ is a suitable matrix. Let us consider that $\mathbf{D}^k$ is positive definite. Multiply Eqn. (16) by ∇f^k yields

$$\mathbf{p}^k \cdot \nabla f^k = - \left(\mathbf{D}^k \cdot \nabla f^k\right) \cdot \nabla f^k < 0 \tag{17}$$

Thus, the positive definiteness of $\mathbf{D}^k$ guarantee a descent direction of $\mathbf{p}^k$. The methods of computation of the matrix $\mathbf{D}^k$ will be discussed in following sections. Note that for $\mathbf{D}^k = \left(\mathbf{H}^k\right)^{-1}$ and $t^k = 1$ one can obtain the Newton-Raphson method. We now turn attention to

the choice of the step length parameter t^k. Its computation is based on the restriction of the minimized function $f(\mathbf{x})$ to the ray from a point $\mathbf{x}^k$ in the search direction $\mathbf{p}^k$

$$\varphi(t) = f\left(\mathbf{x}^k + t\mathbf{p}^k\right), \quad t > 0 \tag{18}$$

Apparently, the exact minimization of this function is computationally expensive. In order to find even a local minimizer of $\varphi(t)$ it generally requires too many evaluations of the minimized function $f(\mathbf{x})$. In Ref. [8], more sophisticated strategies are mentioned to perform an inexact line search to identify a step length that achieves reductions of $f(\mathbf{x})$. In proposed algorithm the step length is computed analytically by the one-dimensional minimizer of the quadratic function along the direction $\mathbf{x}^k + t\mathbf{p}^k$

$$t^k = -\frac{\nabla f^k \cdot \mathbf{p}^k}{(\mathbf{p}^k \cdot \mathbf{H}^k) \cdot \mathbf{p}^k} \tag{19}$$

3.4 Steepest descent method

The steepest descent method is the simplest line search method, for which $\mathbf{D}^k$ is the identity matrix and so the search direction $\mathbf{p}^k$ is the negative gradient. Thus, the iteration scheme is

$$\mathbf{x}^{k+1} = \mathbf{x}^k - t^k \nabla f^k \tag{20}$$

Since the Hessian matrix is not employed the steepest descent method does not converge to the saddle points.

3.5 Broyden's method

The Broyden's method is a generalization of the 1D secant method to multiple dimensions as well as the Newton-Raphson is a generalization of the Newton's tangent method. The Broyden's sequence $\left\{\mathbf{x}^k\right\}$ is defined by the recurrent formula [9]

$$\mathbf{x}^{k+1} = \mathbf{x}^k - t^k \left(\mathbf{D}^k\right)^{-1} \nabla f^k \tag{21}$$

where the update of $\mathbf{D}^k$ is computed by

$$\mathbf{D}^{k+1} = \mathbf{D}^k + \frac{\left(\nabla f^{k+1} - \nabla f^k\right) - \mathbf{D}^k\left(\mathbf{x}^{k+1} - \mathbf{x}^k\right)}{\left(\mathbf{x}^{k+1} - \mathbf{x}^k\right) \cdot \left(\mathbf{x}^{k+1} - \mathbf{x}^k\right)} \otimes \left(\mathbf{x}^{k+1} - \mathbf{x}^k\right) \tag{22}$$

3.6 BFGS method

A very effective minimization method is the Broyden-Fletcher-Goldfarb-Shenno (BFGS) method. This method requires no evaluation of the Hessian matrix. Moreover, the BFGS method was developed so that the search direction $\mathbf{p}^k$ has always a descent direction. Thus, the positive definiteness of the matrix $\mathbf{D}^k$ is guaranteed. The BFGS iteration scheme is defined by the recurrence [9]

$$\mathbf{x}^{k+1} = \mathbf{x}^k - t^k \left(\mathbf{D}^k\right)^{-1} \nabla f^k \tag{23}$$

The update of $\mathbf{D}^k$ is computed by

$$\mathbf{D}^{k+1} = \mathbf{D}^k + \frac{\mathbf{y}^k \otimes \mathbf{y}^k}{\mathbf{d}^k \cdot \mathbf{y}^k} - \frac{\mathbf{D}^k\mathbf{d}^k \otimes \mathbf{D}^k\mathbf{d}^k}{\mathbf{d}^k \cdot \mathbf{D}^k\mathbf{d}^k} \tag{24}$$

where $\mathbf{d}^k = \mathbf{x}^{k+1} - \mathbf{x}^k$ and $\mathbf{y}^k = \nabla f^{k+1} - \nabla f^k$.

3.7 DFP method

Another famous method is the Davidon-Fletcher-Powell (DFP) method. Instead of updating the matrices $\mathbf{D}^k$

$$\mathbf{x}^{k+1} = \mathbf{x}^k - t^k \left(\mathbf{D}^k\right)^{-1} \nabla f^k \tag{25}$$

as in the BFGS method, the DFP method updates their inverses and retains the features of a secant method. The DFP method sequence $\left\{\mathbf{x}^k\right\}$ is defined by the recurrent formula

$$\mathbf{x}^{k+1} = \mathbf{x}^k - t^k \mathbf{D}^k \nabla f^k \tag{26}$$

The update of $\mathbf{D}^k$ is computed by

$$\mathbf{D}^{k+1} = \mathbf{D}^k + \frac{\mathbf{d}^k \otimes \mathbf{d}^k}{\mathbf{y}^k \cdot \mathbf{d}^k} - \frac{\mathbf{D}^k \mathbf{y}^k \otimes \mathbf{D}^k \mathbf{y}^k}{\mathbf{y}^k \cdot \mathbf{D}^k \mathbf{y}^k} \tag{27}$$

where $\mathbf{d}^k = \mathbf{x}^{k+1} - \mathbf{x}^k$, $\mathbf{y}^k = \nabla f^{k+1} - \nabla f^k$.

3.8 Nelder-Mead simplex method

In geometry context, the simplex is a generalization of the motion of a triangle or tetrahedron to arbitrary dimension. Specifically, an n-simplex is an n-dimensional polytope with $n + 1$ vertices whereas the distance between each of them is equal. The examples of such a simplex is shown in Fig. 2. The minimized function is evaluated in all vertices of simplex. The algorithm

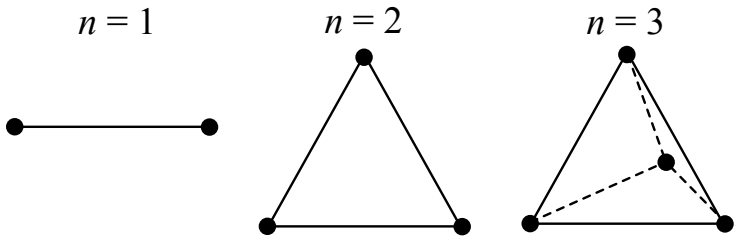

Figure 2: The examples of simplex.

of the simplex method is based on the three rules [10]. The first rule says that the vertex with the maximum value is released. Alternatively, it is replaced by new one according to Fig. 3. In

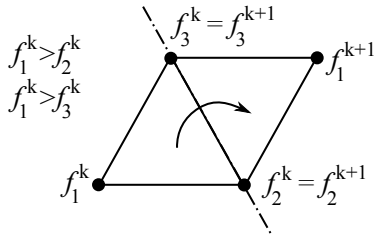

Figure 3: First rule of the simplex method.

case that the value in new vertex is maximum again, the second rule (see Fig. 4) holds. It is not allowed to return the vertex back in the subsequent iteration due to runaway loop. Instead, the

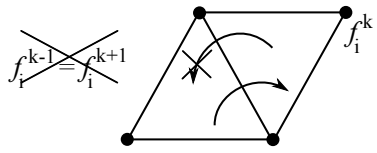

Figure 4: Second rule of the simplex method.

vertex with second highest value is released. Finally, the third rule treats the case when one of the vertices has still the same position. This situation indicates that the simplex rotates above a local extremum. Therefore, the simplex edge length a is halved after m iterations. The number of iteration m can be estimated by the empiric formula

$$m = 1.65n + 0.05n^2 \tag{28}$$

where n is the number of dimensions. Fig. 5 shows two-dimensional case ($n = 2$).

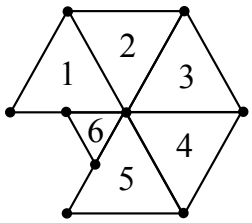

Figure 5: Third rule of the simplex method.

3.9 Comparison of methods for local contact search

A numerical test was performed for three different positions of slave point with respect to the deformed master segment topology. The first estimation was gained by one iteration of the least squares projection. Then, the origin of isoparametric coordinates was taken. Finally, the corners of the master segment were tested as the initial guesses. The results are summarized in Tab. 1, where the number of iterations n and normalized time t are shown. The normalized time is defined as the CPU time related to CPU time for the Newton-Raphson for the initial guess (0.83,-0.62). The criterion of convergence was set $\left\|\mathbf{x}^k - \mathbf{x}^{k-1}\right\| \leq 10^{-10}$. Note that the superscript *sp* denotes the solutions which converged to a saddle point.

	Initial guess											
	(0.83,-0.62)		(0,0)		(-1,-1)		(1,-1)		(1,1)		(-1,1)	
	n	t	n	t	n	t	n	t	n	t	n	t
N-R	28	1.00	5	0.20	12	0.45	17^{sp}	0.61	5^{sp}	0.20	12^{sp}	0.44
LSP	133	0.44	134	0.45	137	0.46	124	0.42	116	0.39	134	0.46
SD	51	4.50	71	6.10	28	2.52	14	1.22	29	2.60	1543	142.97
Broyden	9	0.48	11	0.58	10	0.51	9	0.46	11^{sp}	0.55	14900	819.15
BFGS	8	0.37	8	0.42	8	0.41	7	0.36	9^{sp}	0.48	23	1.22
DFP	7	0.35	8	0.39	8	0.40	7	0.36	9^{sp}	0.45	26	1.28
Simplex	190	6.75	200	7.13	192	6.75	184	6.84	210	7.61	196	6.91

Table 1: n - number of iteration, t - normalized CPU time.

It clear that the best results were obtained for BFGS and DFP methods. The Broyden's as well as the steepest descent methods gave only average results. Due to facts mentioned in Section 3.2 the least squares projection was not efficient for the solution of this problem. In comparison to other methods the advantage of the Nelder-Mead simplex method is insensitivity to the convergence to saddle points. Finally, it should be pointed out that the convergence property of the Newton-Raphson iteration was difficult to achieve in general. It is illustrated by the difference between NR iterations for the first and the second initial point.

In conclusion, the most fitting turned out the conjunction of the simplex method for coarse searching and the quasi-Newton solvers BFGS or DFP for fine tuning of numerical solution. The performance of new local contact search procedure was tested by means of a contact-impact problem of two colliding thick plates. The results are presented in following Section 4.

4 LONGITUDINAL IMPACT OF THICK PLATES

The longitudinal impact of two thick plates was studied, for which the analytical solution was available [12]. Despite the problem is two-dimensional one it could be used for testing three-dimensional local contact search procedure. The plates dimensions were: thickness $2d = 5$ mm, length 2.5 mm. Young's modulus, Poisson's ratio and density, respectively, were $E = 2.1 \times 10^5$ MPa, $\nu = 0.3$, $\rho = 7800\,\mathrm{kg/m^3}$. The plates made contact with initial velocity $v_0 = 1$ m/s prescribed at time $t = 0$ s (Fig. 6).

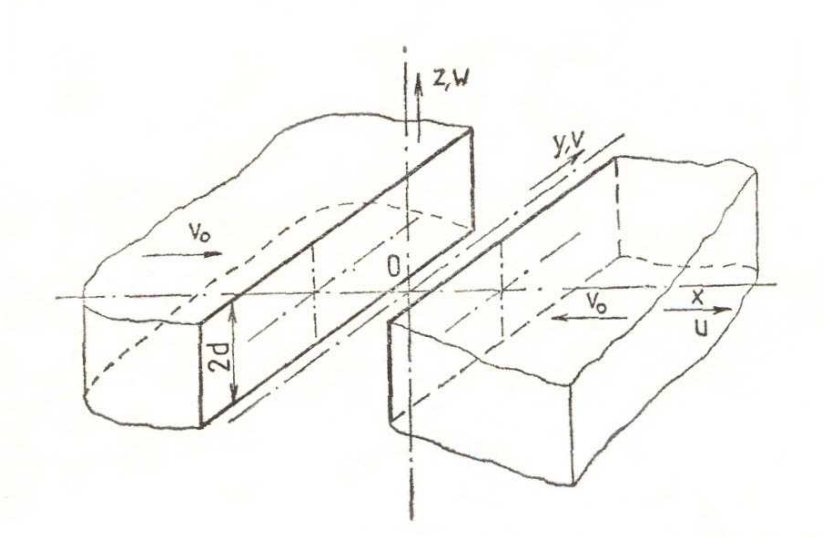

Figure 6: Longitudinal impact of two plates.

The analytical solution [12] utilizing the Laplace transform is rather complex. The distributions of displacements and stresses are cast in the form of infinite series of improper integrals which are evaluated numerically. For illustration, theoretical positions of wave fronts for a short time after impact are plotted in Fig. 7. At the instant the faces of the plates come into contact there are aroused elementary dilatation waves at all points of the contact area. The envelope of these waves is represented by a wave with a plane wave front, propagating in both directions at speed of dilatation waves c_1. From the boundary points A, D of the contact area emanates a reflected wave which continues propagating in perpendicular direction to x, y plane at speed c_1. Behind the dilatation wave the transversal waves proceeds at speed c_2. In the region bounded by plane wave fronts of the dilatation wave and by circular wave fronts of the wave starting from

the points A and D, the state of stress is the same as that encountered by a longitudinal impact of half-spaces.

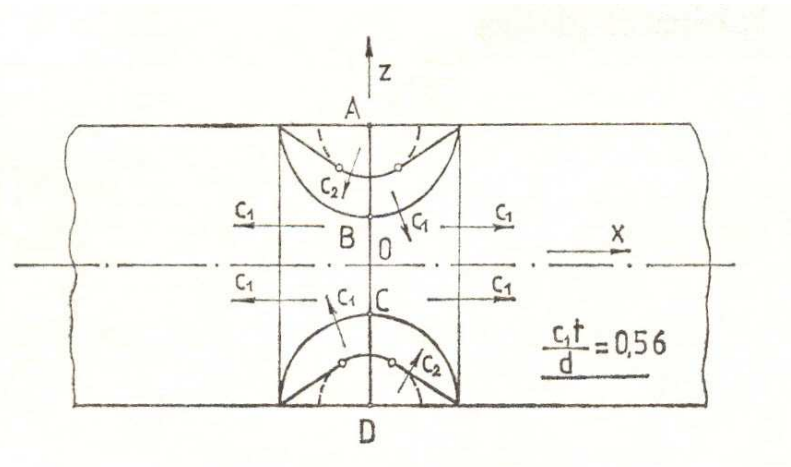

Figure 7: Theoretical position of wave fronts for $c_1 t/d = 0.56$ after [12].

In view of symmetry, only one half of the plates was discretized using 100×100 eight-node linear brick elements per each plate. For the integration of equilibrium equations, the central difference with the lumped mass matrix was employed. The time step was chosen very small corresponding to the dimensionless Courant number C$o = 0.125$.

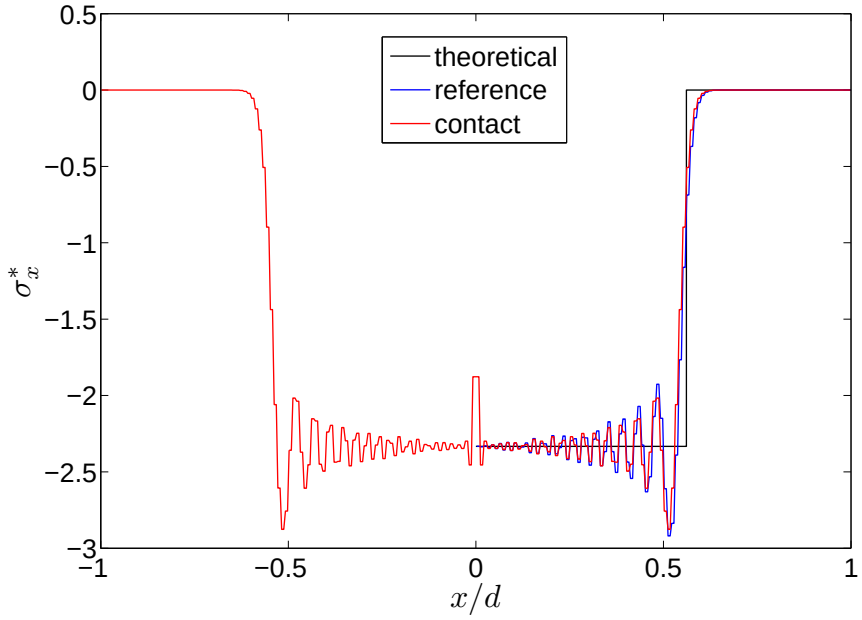

Figure 8: Longitudinal stress distribution σ_x^* along x-axis for $z/d = 0$.

The normalized longitudinal stress distribution $\sigma_x^* = \sigma_x c_1/\Lambda v_0$ (Λ is Lamé's constant) along x-axis is drawn in Fig. 8. The results are plotted for normalized time $c_1 t/d = 0.56$ and coordinate $z/d = 0$, for which no reflections from boundaries occur. Except the contact analysis a symmetric reference calculation was performed, where the longitudinal displacements of the

front-end nodes of the plate were fixed. In Fig. 8 the contact solution is plotted by red line while the solution based on the reference calculation is denoted by blue line. In addition, the theoretical solution corresponding to uniaxial strain condition is plotted by the black line in Fig. 8. It is clear that the numerical solution is influenced by dispersion errors caused by both FE spatial and time discretization. In comparions with the continuum solution the speed of the longitudinal wave is slower. This fact follows from the theoretical dispersion diagrams for the bilinear four-node and serendipity elements (e.g. Ref. [13]). Quite a good agreement between the contact and reference calculation was observed. Furthermore, it should be emphasized that the symmetry of longitudinal stress distributions was perfectly preserved in contact analysis.

The normalized transversal stress distribution $\sigma_z^* = \sigma_z c_1/\Lambda v_0$ along z-axis is drawn in Fig. 9. In contrast to graphs in previous Fig. 8 these distributions are strongly influenced by the longitudinal and transversal waves reflected from the boundary of plate. Before the arrival of these waves the solution is identical to the constant values $\sigma_z^* = -1$ corresponding to a half-space impact problem. Quite a good agreement between the contact and reference calculation versus the analytical solution was observed. It should be pointed out that the accuracy of analytical solution is strongly influenced by the number of terms included in the series of improper integrals [12]. The analytical solution plotted in this paper was derived from the summation of the first 300 terms of this series.

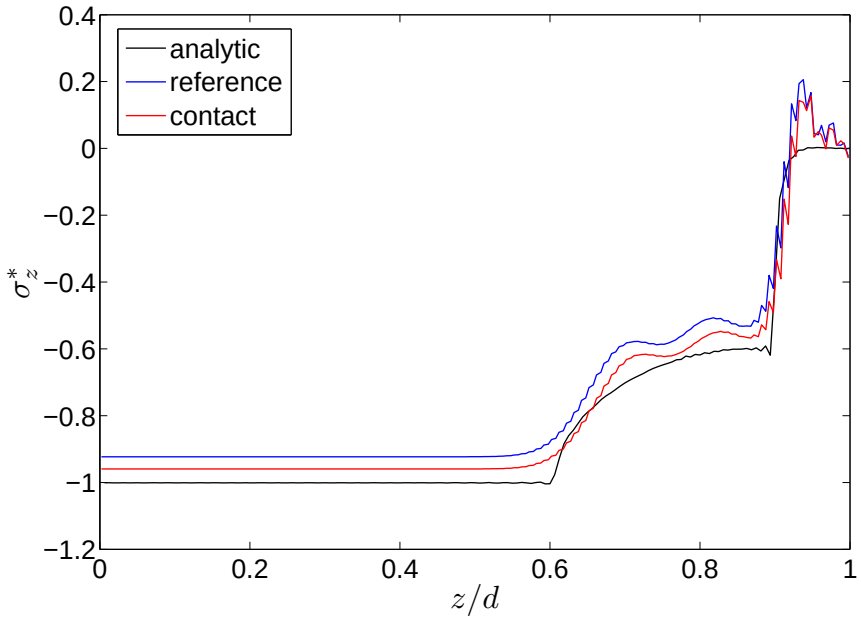

Figure 9: Transversal stress distribution σ_z^* along z-axis for $x/d = 0.4$.

ACKNOWLEDGEMENTS

This work was supported by projects ME10114, GA101/07/1471 and GA101/09/1630 in the framework of AV0Z20760514.

REFERENCES

[1] D. Gabriel, J. Plešek, M. Ulbin, Symmetry preserving algorithm for large displecement frictionless contact by the pre-discretization penalty method. *Int. J. Num. Met. Engng*, **61**, 2615–2638, 2004.

[2] F. Wang, J. Cheng, Z. Yao, FFS contact searching algorithm for dynamic finite element analysis. *Int. J. Num. Met. Engng*, **52**, 655–672, 2001.

[3] J. O. Hallquist, G.L. Goudreau, D. J. Benson, Sliding interfaces with contact-impact in large-scale Lagrangian computations. *Computer Methods in Applied Mechanics and Engineering*, **51**, 107–137, 1985.

[4] A. B. Chaudhary, K.J. Bathe, A solution method for static and dynamic analysis of three-dimensional contact problems with friction. *Computers and Structures*, **24**(6), 855–873, 1986.

[5] D. J. Benson, J. O. Hallquist, A single surface contact algorithm for the post-buckling analysis of shall structures. *Computer Methods in Applied Mechanics and Engineering*, **78**, 141–163, 1990.

[6] Y. T. Keum, E. Nakamachi, R. H. Wagoner, J. K. Lee, Compatible description of tool surfaces and FEM meshes for analysing sheet forming operations. *Int. J. Num. Met. Engng*, **30**(8), 1471–1502, 1990.

[7] S. P. Wang, E. Nakamachi, The inside-outside contact search algorithm for finite element analysis. *Int. J. Num. Met. Engng*, **40**, 3665–3685, 1997.

[8] J. Nocedal, S. J. Wright, *Numerical optimization*. Springer, 1999.

[9] A. L. Peressini, F. E. Sullivan, J. J. Uhl, Jr., *The mathematics of nonlinear programming*. Springer, 1988.

[10] J. A. Nelder, R. Mead, A simplex method for function minimization. *The Computer Journal*, **7**, 308–313, 1965.

[11] J. Kopačka, D. Gabriel, J. Plešek, Review of methods for local contact search. *3rd GACM Colloquium on Computational Mechanics (GACM 2009)*, Hannover, September 20-23, 2009.

[12] R. Brepta, F. Valeš, Longitudinal impact of bodies. *Acta Technica ČSAV*, **32**, 575–602, 1987.

[13] D. Gabriel, J. Plešek, R. Kolman, F. Valeš, M. Ulbin, Two benchmark problems for testing accuracy and stability of finite element solutions to wave propagation. M. Papadrakakis et al. eds., *COMPDYN 2009*, ECCOMAS 2009.